Chapter 6

Modal Phenomena of Surface and Bulk Polaritons in Magnetic-Semiconductor Superlattices

Vladimir R. Tuz, Illia V. Fedorin and Volodymyr I. Fesenko

Additional information is available at the end of the chapter

http://dx.doi.org/10.5772/intechopen.71837

Abstract

We discuss peculiarities of bulk and surface polaritons propagating in a composite magnetic-semiconductor superlattice influenced by an external static magnetic field. Three particular configurations of magnetization, namely, the Voigt, polar, and Faraday geometries, are considered. In the long-wavelength limit, involving the effective medium theory, the proposed superlattice is described as an anisotropic uniform medium defined by the tensors of effective permittivity and effective permeability. The study is carried out in the frequency band where the characteristic resonant frequencies of underlying constitutive magnetic and semiconductor materials of the superlattice are different but closely spaced. The effects of mode crossing and anti-crossing in dispersion characteristics of both bulk and surface polaritons are revealed and explained with an assistance of the concept of Morse critical points from the catastrophe theory.

Keywords: electromagnetic theory, polaritons, magneto-optical materials, superlattices, metamaterials

1. Introduction

Surface polaritons are a special type of electromagnetic waves propagating along the interface of two partnering materials whose material functions (e.g., permittivities) have opposite signs that are typical for a metal-dielectric boundary [1]. These waves are strongly localized at the interface and penetrate into the surrounding space over a distance of wavelength order in a medium, and their amplitudes fall exponentially away from the surface. Observed strong confinement of electromagnetic field in small volumes beyond the diffraction limit leads to enormous increasing matter-field interaction, and it makes attractive using surface waves in the wide fields from the microwave and photonic devices to solar cells [2, 3]. Furthermore, surface electromagnetic waves are highly promising from physical point of view because from

the character of their propagation, one can derive information about both interface quality and electromagnetic properties of partnering materials (such as permittivity and permeability). High sensitivity to the electromagnetic properties of media enables utilization of surface waves in the sensing applications, particularly in both chemical and biological systems [4]. Thus, studying characteristics of surface waves is essential in the physics of surfaces and optics; in the latter case, the research has led to the emergence of a new science—plasmonics.

Today plasmonics is a rapidly developing field characterized by enormous variety of possible practical applications. In many of them, an ability to control and guide surface waves is a crucial characteristic. Thereby in last decades, many efforts have been made to realize active tunable components for plasmonic integrated circuits such as switchers, active couplers, modulators, etc. In this regard, searching effective ways to control characteristics of plasmon-polariton propagation by utilizing external driving agents is a very important task. In particular, the nonlinear, thermo-optical, and electro-optical effects are proposed to be used in the tunable plasmonic devices for the control of plasmon-polariton propagation [5–8]. In such devices, the tuning mechanism is conditioned by changing the permittivity of the dielectric medium due to applying external electric field or temperature control. At the same time, utilization of an external magnetic field as a driving agent to gain a control over polariton dispersion features is very promising, since it allows changing both permeability of magnetic materials (e.g., ferrites) and permittivity of conducting materials (e.g., metals or semiconductors). It is worth mentioning that the uniqueness of this controlling mechanism lies in the fact that the polariton properties depend not only on the magnitude of the magnetic field but also on its direction. An applied magnetic field also produces additional branches in spectra of magnetic plasmon-polariton resulting in the multiband propagation accompanied by nonreciprocal effects [9–16]. Thus, a combination of plasmonic and magnetic functionalities opens a prospect toward active devices with an additional degrees of freedom in the control of plasmon-polariton properties, and such systems have already found a number of practical applications in integrated photonic devices for telecommunications (see, for instance [3, 8] and references therein).

In this framework, using superlattices (which typically consist of alternating layers of two partnering materials) that are capable to provide a combined plasmon and magnetic functionality instead of traditional plasmonic systems (in which the presence of a metal-dielectric interface is implied) has great prospects. Particularly, it conditioned by the fact that the superlattices demonstrate many exotic electronic and optical properties uncommon to the homogeneous (bulk) samples due to the presence of additional periodic potential, which period is greater than the original lattice constant [14]. The application of magnetic field to a superlattice leads to the so-called magneto-plasmon-polariton excitations. Properties of the magnetic polaritons in the superlattices of different kinds being under the action of an external static magnetic field have been studied by many authors during several last decades [10–16]. The problem is usually solved within two distinct considerations of gyroelectric media (e.g., semiconductors) with magneto-plasmons [10, 14] and gyromagnetic media (e.g., ferrites) with magnons [11–13, 16], which involve the medium characterization with either permittivity or permeability tensor having asymmetric off-diagonal parts. This distinction is governed by the fact that the resonant frequencies of permeability of magnetic materials usually lie in the

http://dx.doi.org/10.5772/intechopen.71837

microwave range, whereas characteristic frequencies of permittivity of semiconductors commonly are in the infrared range.

At the same time, it is evident that combining together magnetic and semiconductor materials into a single gyroelectromagnetic superlattice in which both permeability and permittivity simultaneously are tensor quantities allows additional possibilities in the control of polaritons using the magnetic field that are unattainable in convenient either gyromagnetic or gyroelectric media. Fortunately, it is possible to design heterostructures in which both characteristic resonant frequencies of semiconductor and magnetic materials are different but, nevertheless, closely spaced in the same frequency band. As a relevant example, the magnetic-semiconductor heterostructures proposed in [17–20] can be mentioned that are able to exhibit a gyroelectromagnetic effect from gigahertz up to tens of terahertz [21]. Thus investigation of electromagnetic properties of such structures in view of their promising application as a part of plasmonic devices is a significant task.

This chapter is devoted to the discussion of dispersion peculiarities of both bulk and surface polaritons propagating in a finely-stratified magnetic-semiconductor superlattice influenced by an external static magnetic field. It is organized as follows. In Section 2, we formulate the problem to be solved and derive effective medium expressions suitable for calculation of the properties of modes under the long-wavelength approximation. Section 3 describes the problem solution in a general case assuming an arbitrary orientation of the external magnetic field with respect to the direction of wave propagation and interface of the structure. The discussion about manifestation of mode crossing and anti-crossing effects is presented in Section 4 involving a concept of the Morse critical points from the catastrophe theory. In Section 5, we reveal dispersion peculiarities of bulk and surface polaritons in the given superlattice for three particular cases of the vector orientation of the external magnetic field with respect to the superlattice's interface and wave vector, namely we study the configurations where the external magnetic field is influenced in the Voigt, polar, and Faraday geometries. Finally, Section 6 summarizes the chapter.

2. Outline of problem

Thereby, in this chapter, we study dispersion features of surface and bulk polaritons propagating in a *semi-infinite* stack of identical composite double-layered slabs arranged along the y-axis that forms a *superlattice* (**Figure 1**). Each composite slab within the superlattice includes magnetic (with constitutive parameters ε_m, $\widehat{\mu}_m$) and semiconductor (with constitutive parameters $\widehat{\varepsilon}_s$, μ_s) layers with thicknesses d_m and d_s, respectively. The stack possesses a periodic structure (with period $L = d_m + d_s$) that fills half-space $y < 0$ and adjoins a vacuum $\left(\varepsilon_0 = \mu_0 = 1\right)$ occupying half-space $y > 0$. Therefore, the superlattice's interface lies in the $x - z$ plane, and along this plane, the system is considered to be infinite. The structure under investigation is influenced by an external static magnetic field $\vec{M}$ that lies in the $y - z$ plane and makes an angle θ with the y-axis. It is supposed that the strength of this field is high enough to form a homogeneous saturated state of magnetic as well as semiconductor subsystems. Finally, the

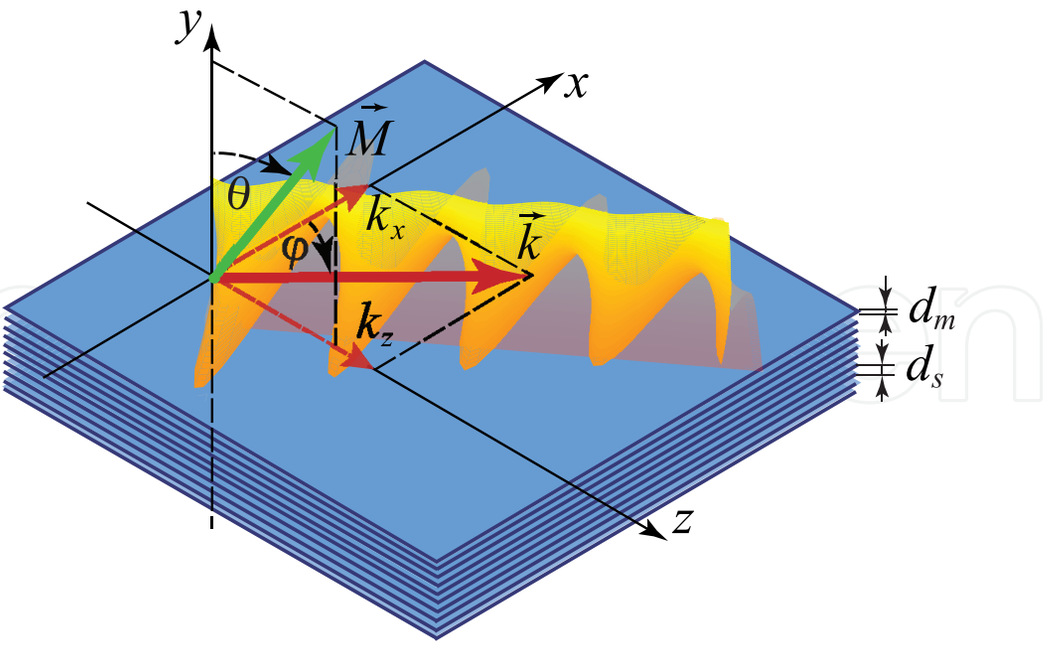

Figure 1. Schematic representation of a magnetic-semiconductor superlattice influenced by an external static magnetic field $\vec{M}$ and a visual representation of the tangential electric field distribution of the surface polariton propagating over the interface between the given structure and free space.

wave vector $\vec{k}$ of the macroscopic electric field lies in the $x-z$ plane and makes an angle φ with the x-axis.

In the general case, when no restrictions are imposed on characteristic dimensions (d_m, d_s, and L) of the superlattice compared to the wavelength of propagating modes, the transfer matrix formalism [22] is usually involved in order to reveal the dispersion features of polaritons. It implies a *numerical* solution of a canonical boundary value problem formulated for each layer within the period of superlattice and then performing a subsequent multiplication of the obtained transfer matrices to form a semi-infinite extent. On the other hand, when all characteristic dimensions of the superlattice satisfy the long-wavelength limit, i.e., they are all much smaller than the wavelength in the corresponding layer and period of structure ($d_m \ll \lambda$, $d_s \ll \lambda$, $L \ll \lambda$), homogenization procedures from the effective medium theory can be involved in order to derive dispersion characteristics in an *explicit* form [24–28] that is suitable for identifying the main features of interest. Therefore, further only the modes under the long-wavelength approximation are studied in this chapter, i.e., the structure is considered to be a *finely-stratified* one.

In order to obtain expressions for the tensors of effective permeability and permittivity of the superlattice in a general form, constitutive equations, $\vec{B}=\mu\vec{H}$ and $\vec{D}=\varepsilon\vec{E}$, for magnetic ($0<z<d_m$) and semiconductor ($d_m<z<L$) layers are represented as follow [26]:

$$Q_\nu^{(j)} = \sum_{\nu'} g_{\nu\nu'}^{(j)} P_{\nu'}^{(j)}, \tag{1}$$

where $\vec{Q}$ takes values of the magnetic and electric flux densities $\vec{B}$ and $\vec{D}$, respectively; $\vec{P}$ is varied between the magnetic and electric field strengths $\vec{H}$ and $\vec{E}$; g is substituted for

http://dx.doi.org/10.5772/intechopen.71837

permeability and permittivity μ and ε; the superscript j is introduced to distinguish between magnetic ($m \to j$) and semiconductor ($s \to j$) layers; and $\nu\nu'$ iterates over x, y, and z.

In the given structure geometry, the interfaces between adjacent layers within the superlattice lie in the $x - z$ plane, and they are normal to the y-axis; thus, the field components $P_x^{(j)}$, $P_z^{(j)}$, and $Q_y^{(j)}$ are continuous at the interfaces. Therefore, the normal component $P_y^{(j)}$ can be expressed from (1) in terms of the continuous components of the field as follow:

$$P_y^{(j)} = -\frac{g_{yx}^{(j)}}{g_{yy}^{(j)}} P_x^{(j)} + \frac{1}{g_{yy}^{(j)}} Q_y^{(j)} - \frac{g_{yz}^{(j)}}{g_{yy}^{(j)}} P_z^{(j)}, \tag{2}$$

and substituted into equations for components $Q_x^{(j)}$ and $Q_z^{(j)}$:

$$\begin{aligned} Q_x^{(j)} &= \left(g_{xx}^{(j)} - \frac{g_{xy}^{(j)} g_{yx}^{(j)}}{g_{yy}^{(j)}} \right) P_x^{(j)} + \frac{g_{xy}^{(j)}}{g_{yy}^{(j)}} Q_y^{(j)} + \left(g_{xz}^{(j)} - \frac{g_{xy}^{(j)} g_{yz}^{(j)}}{g_{yy}^{(j)}} \right) P_z^{(j)} \\ Q_z^{(j)} &= \left(g_{zx}^{(j)} - \frac{g_{zy}^{(j)} g_{yx}^{(j)}}{g_{yy}^{(j)}} \right) P_x^{(j)} + \frac{g_{zy}^{(j)}}{g_{yy}^{(j)}} Q_y^{(j)} + \left(g_{zz}^{(j)} - \frac{g_{zy}^{(j)} g_{yz}^{(j)}}{g_{yy}^{(j)}} \right) P_z^{(j)}. \end{aligned}, \tag{3}$$

Relations (2) and (3) are then used for the field averaging [24].

With taking into account the long-wavelength limit, the fields $\vec{P}(j)$ and $\vec{Q}(j)$ inside the layers are considered to be constant, and the *averaged* (Maxwell) fields $\left\langle \vec{Q} \right\rangle$ and $\left\langle \vec{P} \right\rangle$ can be determined by the equalities:

$$\left\langle \vec{P} \right\rangle = \frac{1}{L} \sum_j \vec{P}\,(j) d_j, \quad \left\langle \vec{Q} \right\rangle = \frac{1}{L} \sum_j \vec{Q}\,(j) d_j. \tag{4}$$

In view of the continuity of components $P_x^{(j)}$, $P_z^{(j)}$, and $Q_y^{(j)}$, it follows that

$$\langle P_x \rangle = P_x^{(j)}, \quad \langle P_z \rangle = P_z^{(j)}, \quad \left\langle Q_y \right\rangle = Q_y^{(j)}, \tag{5}$$

and with using Eqs. (2) and (3), we can obtain the relations between the averaged field components in the next form:

$$\begin{aligned} \langle Q_x \rangle &= \alpha_{xx} \langle P_x \rangle + \gamma_{xy} \left\langle Q_y \right\rangle + \alpha_{xz} \langle P_z \rangle, \\ \left\langle P_y \right\rangle &= \beta_{yx} \langle P_x \rangle + \beta_{yy} \left\langle Q_y \right\rangle + \beta_{yz} \langle P_z \rangle, \\ \langle Q_z \rangle &= \alpha_{zz} \langle P_x \rangle + \gamma_{zy} \left\langle Q_y \right\rangle + \alpha_{zz} \langle P_z \rangle. \end{aligned} \tag{6}$$

Here, we used the following designations $\alpha_{\nu\nu'} = \sum_j \left(g_{\nu\nu'}^{(j)} - g_{\nu y}^{(j)} g_{y\nu'}^{(j)} / g_{yy}^{(j)} \right) \delta_j$, $\beta_{yy} = \sum_j \left(1/g_{yy}^{(j)} \right) \delta_j$, $\beta_{yy} = \sum_j \left(g_{y\nu'}^{(j)} / g_{yy}^{(j)} \right) \delta_j$, $\gamma_{\nu y} = \sum_j \left(g_{\nu y}^{(j)} / g_{yy}^{(j)} \right) \delta_j$, $\delta_j = d_j / L$ is filling factor, and $\nu\nu'$ iterates over x and z.

Expressing $\left\langle Q_y \right\rangle$ from the second equation in system (6) and substituting it into the rest two equations, the constitutive equations for the flux densities of the effective medium $\left\langle \vec{Q} \right\rangle = \hat{g}_{eff} \left\langle \vec{P} \right\rangle$ can be derived, where $\hat{g}_{eff}$ is a tensor quantity:

$$\hat{g}_{eff} = \begin{pmatrix} \tilde{\alpha}_{xx} & \tilde{\gamma}_{xy} & \tilde{\alpha}_{xz} \\ \tilde{\beta}_{yx} & \tilde{\beta}_{yy} & \tilde{\beta}_{yz} \\ \tilde{\alpha}_{zx} & \tilde{\gamma}_{zy} & \tilde{\alpha}_{zz} \end{pmatrix} = \begin{pmatrix} \tilde{g}_{xx} & \tilde{g}_{xy} & \tilde{g}_{xz} \\ \tilde{g}_{yx} & \tilde{g}_{yy} & \tilde{g}_{yz} \\ \tilde{g}_{zx} & \tilde{g}_{zy} & \tilde{g}_{zz} \end{pmatrix}, \tag{7}$$

with components $\tilde{\alpha}_{\nu\nu'} = \alpha_{\nu\nu'} - \beta_{y\nu'}\gamma_{\nu y}/\beta_{yy}$, $\tilde{\beta}_{yy} = 1/\tilde{\beta}_{yy}$, $\tilde{\beta}_{y\nu'} = -\beta_{y\nu'}/\beta_{yy}$, and $\tilde{\gamma}_{\nu y} = -\gamma_{\nu y}/\beta_{yy}$.

The expressions for tensor components of the underlying constitutive parameters of magnetic ($\hat{\mu}_m \to \hat{g}^{(m)}$) and semiconductor ($\hat{\varepsilon}_s \to \hat{g}^{(s)}$) layers depend on the orientation of the external magnetic field $\vec{M}$ in the $y-z$ plane which is defined by the angle θ in the form:

$$\hat{g}^{(j)} = \begin{pmatrix} g_1 & i\zeta g_2 & i\xi g_2 \\ -i\zeta g_2 & \zeta^2 g_1 + \xi^2 g_3 & \zeta\xi(g_1 - g_3) \\ -i\xi g_2 & \zeta\xi(g_1 - g_3) & \xi^2 g_1 + \zeta^2 g_3 \end{pmatrix}, \tag{8}$$

where $\zeta = \sin\theta$ and $\xi = \cos\theta$.

For magnetic layers [29], the components of tensor $\hat{g}^{(m)}$ are $g_1 = 1 + \chi' + i\chi''$, $g_2 = \Omega' + i\Omega''$, $g_3 = 1$ and $\chi' = \omega_0\omega_m\left[\omega_0^2 - \omega^2(1-b^2)\right]D^{-1}$, $\chi'' = \omega\omega_m b\left[\omega_0^2 + \omega^2(1+b^2)\right]D^{-1}$, $\Omega' = \omega\omega_m\left[\omega_0^2 - \omega^2(1+b^2)\right]D^{-1}$, $\Omega'' = 2\omega^2\omega_0\omega_m bD^{-1}$, and $D = \left[\omega_0^2 - \omega^2(1+b^2)\right]^2 + 4\omega_0^2\omega b^2$, where ω_0 is the Larmor frequency and b is a dimensionless damping constant.

For semiconductor layers [23], the components of tensor $\hat{g}^{(s)}$ are $g_1 = \varepsilon_l\left[1 - \omega_p^2(\omega + i\nu)[\omega((\omega + i\nu)^2 - \omega_c^2)]^{-1}\right]$, $g_2 = \varepsilon_l\omega_p^2\omega_c\left[\omega\left((\omega + i\nu)^2 - \omega_c^2\right)\right]^{-1}$, and $g_3 = \varepsilon_l\left[1 - \left[\omega_p^2(\omega + i\nu)\right]^{-1}\right]$, where ε_l is the part of permittivity attributed to the lattice, ω_p is the plasma frequency, ω_c is the cyclotron frequency, and ν is the electron collision frequency in plasma.

Permittivity ε_m of the magnetic layers as well as permeability μ_s of the semiconductor layers are scalar quantities.

Hereinafter, we consider two specific orientations of the external magnetic field vector $\vec{M}$ with respect to the superlattice's interface (see **Figure 1**), namely (i) the polar configuration in which $\theta = 0$ and the vector $\vec{M}$ is parallel to the surface normal ($\vec{M} \| y$) and (ii) $\theta = \pi/2$ and the vector $\vec{M}$ is parallel to the surface plane ($\vec{M} \| z$), which is inherent in both the Voigt and Faraday configurations.

http://dx.doi.org/10.5772/intechopen.71837

When $\vec{M} \| y$, then $\zeta = 0$, $\xi = 1$, and tensor (8) is reduced to the form

$$\widehat{g}^{(j)} = \begin{pmatrix} g_1 & 0 & ig_2 \\ 0 & g_3 & 0 \\ -ig_2 & 0 & g_1 \end{pmatrix}, \tag{9}$$

and for the components of tensor (7), we have following expressions: $\tilde{\gamma}_{xy} = \tilde{\gamma}_{zy} = \tilde{\beta}_{yx} = \tilde{\beta}_{yz} = 0$, $\tilde{\alpha}_{xx} = g_{xx}^{(m)}\delta_m + g_{xx}^{(s)}\delta_s$, $\tilde{\alpha}_{zz} = g_{zz}^{(m)}\delta_m + g_{zz}^{(s)}\delta_s$, $\tilde{\alpha}_{xz} = -\tilde{\alpha}_{zx} = g_{zx}^{(m)}\delta_m + g_{zx}^{(s)}\delta_s$, and $\tilde{\beta}_{yy} = g_{yy}^{(m)} g_{yy}^{(s)}\tau$, where $\tau = \left(g_{yy}^{(m)}\delta_s + g_{yy}^{(s)}\delta_m\right)^{-1}$.

In the second case, when $\vec{M} \| z$, then $\zeta = 1$, $\xi = 0$, and tensor (8) has the form

$$\widehat{g}^{(j)} = \begin{pmatrix} g_1 & ig_2 & 0 \\ -ig_2 & g_1 & 0 \\ 0 & 0 & g_3 \end{pmatrix}. \tag{10}$$

In this configuration, the components of tensor (7) can be written as follows: $\tilde{\alpha}_{xz} = \tilde{\alpha}_{zx} = \tilde{\gamma}_{zy} = \tilde{\beta}_{yz} = 0$, $\tilde{\alpha}_{xx} = g_{xx}^{(m)}\delta_m + g_{xx}^{(s)}\delta_s + \left(g_{xy}^{(m)} - g_{xy}^{(s)}\right)^2\delta_m\delta_s\tau$, $\tilde{\alpha}_{zz} = g_{zz}^{(m)}\delta_m + g_{zz}^{(s)}\delta_s$, $\tilde{\gamma}_{xy} = -\tilde{\beta}_{yx} = \left(g_{xy}^{(m)} g_{yy}^{(s)}\delta_m + g_{xy}^{(s)} g_{yy}^{(m)}\delta_s\right)\tau$, and $\tilde{\beta}_{yy} = g_{yy}^{(m)} g_{yy}^{(s)}\tau$.

For further reference, the dispersion curves of the tensor components of relative effective permeability $\widehat{\mu}_{eff}$ and relative effective permittivity $\widehat{\varepsilon}_{eff}$ of the homogenized medium (with filling factors $\delta_m = \delta_s = 0.5$) are presented in **Figure 2**. **Figure 2(a)** and **(b)** represents constitutive parameters for the polar configuration, whereas **Figure 2(c)** and **(d)** represents those for the Voigt and Faraday configurations of magnetization. For these calculations, we used typical constitutive parameters for magnetic and semiconductor materials. In particular, here we follow the results of paper [30], where a magnetic-semiconductor composite is made in the form of a barium-cobalt/doped-silicon superlattice for operating in the microwave part of spectrum. A distinct peculiarity of such a superlattice is that the characteristic resonant frequencies of the underlying constitutive magnetic and semiconductor materials are closely spaced within the same frequency band.

From **Figure 2**, one can conclude that in both the Voigt and Faraday geometries, the next relations between the components of effective tensor (7) hold $\tilde{g}_{xx} \neq \tilde{g}_{yy} \neq \tilde{g}_{zz}$ and $\tilde{g}_{xy} = -\tilde{g}_{yx} \neq 0$, so it means that the obtained homogenized medium is a *biaxial* bigyrotropic crystal [1]. In the polar geometry, it is a *uniaxial* bigyrotropic crystal, and the following relations between tensor components are met: $\tilde{g}_{xx} = \tilde{g}_{zz} \neq \tilde{g}_{yy}$ and $\tilde{g}_{xz} = -\tilde{g}_{zx} \neq 0$.

To sum up, with an assistance of the homogenization procedures from the effective medium theory, the superlattice under study is approximately represented as a uniaxial or biaxial anisotropic uniform medium when an external static magnetic field $\vec{M}$ is directed along or

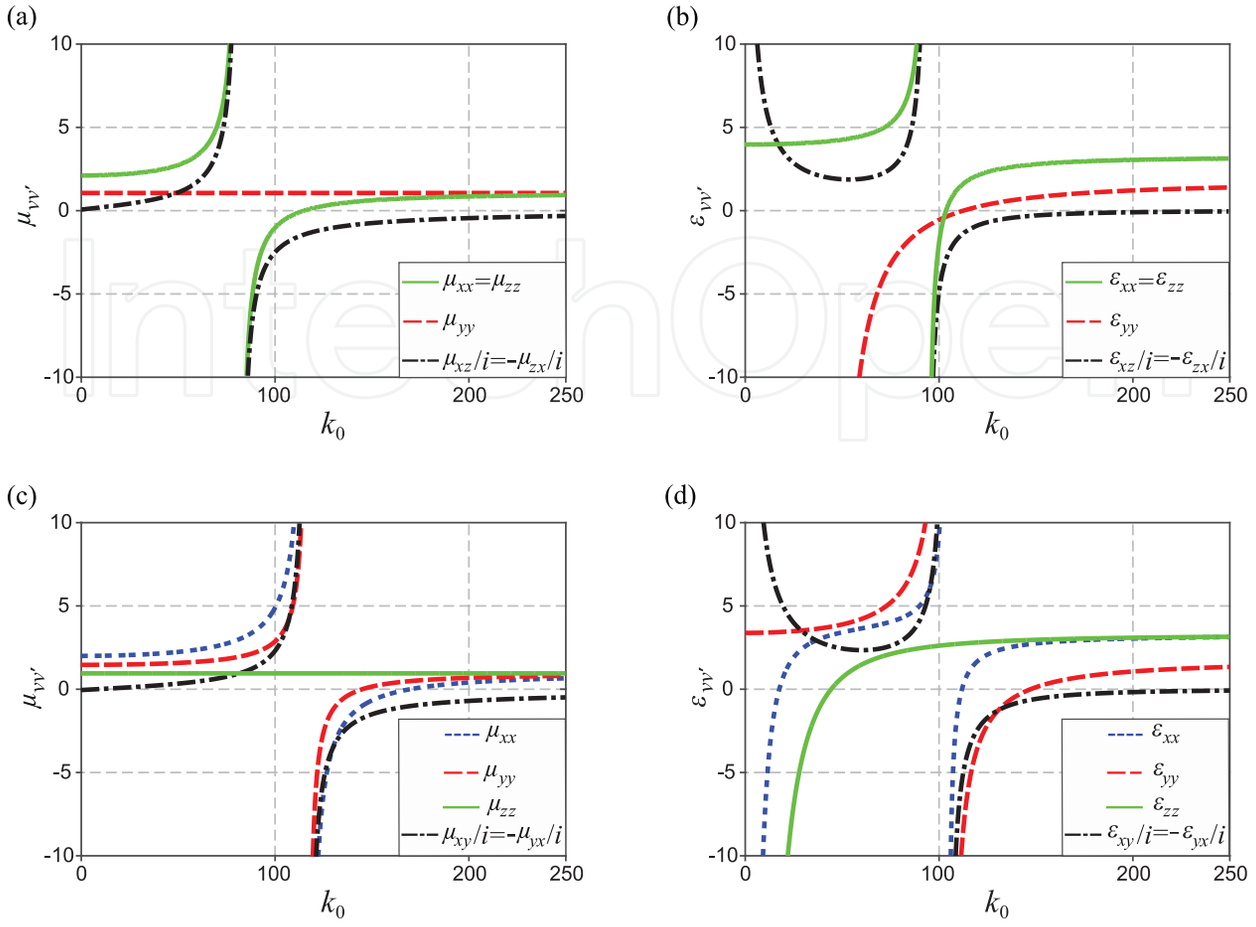

Figure 2. Dispersion curves of the tensor components of (a, c) relative effective permeability $\widehat{\mu}_{eff}$ and (b, d) relative effective permittivity $\widehat{\varepsilon}_{eff}$ of the homogenized medium. Panels (a) and (b) correspond to the polar geometry and panels (c) and (d) correspond to the Voigt and Faraday geometries. For the magnetic constitutive layers, under saturation magnetization of 2930 G, parameters are $f_0 = \omega_0/2\pi = 3.9$ GHz, $f_m = \omega_m/2\pi = 8.2$ GHz, $b = 0$, and $\varepsilon_m = 5.5$; for the semiconductor constitutive layers, parameters are $f_p = \omega_p/2\pi = 5.5$ GHz, $f_c = \omega_c/2\pi = 4.5$ GHz, $\nu = 0$, $\varepsilon_l = 1.0$, and $\mu_s = 1.0$. Filling factors are $\delta_m = \delta_s = 0.5$.

orthogonal to the structure periodicity, respectively. In the latter case, the first optical axis of the biaxial medium is directed along the structure periodicity, whereas the second one coincides with the direction of the external static magnetic field $\vec{M}$.

3. General solution for bulk and surface polaritons

In order to obtain a *general* solution for both bulk and surface polaritons, we follow the approach developed in Ref. [10] where dispersion characteristics of polaritons in a uniaxial anisotropic dielectric medium have been studied. Here, we extend this approach to the case of a gyroelectromagnetic medium whose permittivity and permeability simultaneously are tensor quantities.

http://dx.doi.org/10.5772/intechopen.71837

In a general form [26], the electric and magnetic field vectors $\vec{E}$ and $\vec{H}$ used here are represented as

$$\vec{P}^{(j)} = \vec{p}^{(j)} \exp\left[i(k_x x + k_z z)\right] \exp\left(\mp \kappa y\right), \tag{11}$$

where a time factor $\exp(-i\omega t)$ is also supposed and omitted, and sign $"-"$ is related to the fields in the upper medium ($y > 0,\ j = 0$), while sign $"+"$ is related to the fields in the composite medium ($y < 0,\ j = 1$), respectively, which provide required wave attenuation along the y-axis.

From a pair of the curl Maxwell's equations $\nabla\times \vec{E} = ik_0 \vec{B}$ and $\nabla\times \vec{H} = -ik_0 \vec{D}$, in a standard way, we arrive at the following equation for the macroscopic field:

$$\nabla \times \nabla \times \vec{P}^{(j)} - k_0^2 \widehat{\varsigma}^{(j)} \vec{P}^{(j)} = 0, \tag{12}$$

where $k_0 = \omega/c$ is the free-space wavenumber and $\widehat{\varsigma}^{(j)}$ is introduced as the product of $\widehat{\mu}^{(j)}$ and $\widehat{\varepsilon}^{(j)}$ made in the appropriate order.

For the upper medium ($j = 0$), direct substitution of expression (11) with $\vec{P}^{(0)}$ and corresponding constitutive parameters ($\widehat{\varsigma}^{(0)}_{\nu\nu'} = 1$ for $\nu = \nu'$ and $\widehat{\varsigma}^{(0)}_{\nu\nu'} = 0$ for $\nu \neq \nu'$; here and further subscripts ν and ν' are substituted to iterate over indexes of the tensor components x, y, and z in Cartesian coordinates) into Eq. (12) gives us the relation with respect to κ_0:

$$\kappa_0^2 = k^2 - k_0^2, \tag{13}$$

where $k^2 = k_x^2 + k_z^2$.

For the composite medium ($j = 1$), substitution of (11) with $\vec{P}^{(1)}$ and $\widehat{\varsigma}^{(1)}$ into (12) and subsequent elimination of $P_y^{(1)}$ yield us the following system of two homogeneous algebraic equations for the rest two components of $\vec{P}^{(1)}$:

$$\begin{aligned} A_{xz} P_x^{(1)} + B_{xz} P_z^{(1)} &= 0, \\ B_{zx} P_x^{(1)} + A_{zx} P_z^{(1)} &= 0, \end{aligned} \tag{14}$$

where A_{nm} and B_{nm} are functions of κ derived in the form [10]:

$$\begin{aligned} A_{nm}(\kappa) &= \left(k_m^2 - k_0^2 \varsigma_{nn}^{(1)} - \kappa^2\right) \varkappa_y^2 + k_n^2 \kappa^2 + ik_n \kappa \left(\varsigma_{ny}^{(1)} + \varsigma_{yn}^{(1)}\right) k_0^2 - k_0^4 \varsigma_{ny}^{(1)} \varsigma_{yn}^{(1)}, \\ B_{nm}(\kappa) &= -\left(k_n k_m + \varsigma_{nm}^{(1)}\right) \varkappa_y^2 + k_n k_m \kappa^2 + i\kappa \left(k_n \varsigma_{ym}^{(1)} + k_m \varsigma_{ny}^{(1)}\right) k_0^2 - k_0^4 \varsigma_{ny}^{(1)} \varsigma_{ym}^{(1)}, \end{aligned} \tag{15}$$

with $\varkappa_y^2 = k^2 - k_0^2 \varsigma_{yy}^{(1)}$, and subscripts m and n iterate over indexes x and z.

In order to find a nontrivial solution of system (15), we set its determinant of coefficients to zero. After disclosure of the determinant, we obtain an equation of the fourth degree with respect to κ:

$$\varsigma_{yy}^{(1)}\kappa^4 + a\kappa^3 + b\kappa^2 + c\kappa + d = 0, \tag{16}$$

whose coefficients a, b, c, and d are

$$\begin{aligned}
a &= ik_x\left(\varsigma_{yz}^{(1)} + \varsigma_{zy}^{(1)}\right) + ik_z\left(\varsigma_{yx}^{(1)} + \varsigma_{xy}^{(1)}\right),\\
b &= k_0^2\left[\varsigma_{yy}^{(1)}\left(\varsigma_{zz}^{(1)} + \varsigma_{xx}^{(1)}\right) - \varsigma_{zy}^{(1)}\varsigma_{yz}^{(1)} - \varsigma_{xy}^{(1)}\varsigma_{yx}^{(1)}\right]\\
&\quad -\left[k^2\varsigma_{yy}^{(1)} + k_z^2\varsigma_{zz}^{(1)} + k_x^2\varsigma_{xx}^{(1)} + k_xk_z\left(\varsigma_{zx}^{(1)} + \varsigma_{xz}^{(1)}\right)\right],\\
c &= -ik_0^2\left\{k_z\left[\varsigma_{xy}^{(1)}\varsigma_{zx}^{(1)} + \varsigma_{yx}^{(1)}\varsigma_{xz}^{(1)} - \varsigma_{xx}^{(1)}\left(\varsigma_{yz}^{(1)} + \varsigma_{zy}^{(1)}\right)\right]\right.\\
&\quad \left.+k_x\left[\varsigma_{yz}^{(1)}\varsigma_{zx}^{(1)} + \varsigma_{zy}^{(1)}\varsigma_{xz}^{(1)} - \varsigma_{zz}^{(1)}\left(\varsigma_{yx}^{(1)} + \varsigma_{xy}^{(1)}\right)\right]\right\}\\
&\quad -ik^2\left[k_z\left(\varsigma_{yz}^{(1)} + \varsigma_{zy}^{(1)}\right) + k_x\left(\varsigma_{yx}^{(1)} + \varsigma_{xy}^{(1)}\right)\right],\\
d &= k^2\left[k_z^2\varsigma_{zz}^{(1)} + k_x^2\varsigma_{xx}^{(1)} + k_xk_z\left(\varsigma_{zx}^{(1)} + \varsigma_{xz}^{(1)}\right)\right] + k_0^2k^2\left[\varsigma_{zx}^{(1)}\varsigma_{xz}^{(1)} - \varsigma_{zz}^{(1)}\varsigma_{xx}^{(1)}\right]\\
&\quad +k_0^2\left\{k_x^2\left(\varsigma_{xy}^{(1)}\varsigma_{yx}^{(1)} - \varsigma_{yy}^{(1)}\varsigma_{xx}^{(1)}\right) + k_z^2\left(\varsigma_{zy}^{(1)}\varsigma_{yz}^{(1)} - \varsigma_{yy}^{(1)}\varsigma_{zz}^{(1)}\right)\right.\\
&\quad \left.+k_xk_z\left[\varsigma_{xy}^{(1)}\varsigma_{yz}^{(1)} + \varsigma_{zy}^{(1)}\varsigma_{yx}^{(1)} - \varsigma_{yy}^{(1)}\left(\varsigma_{zx}^{(1)} + \varsigma_{xz}^{(1)}\right)\right]\right\}\\
&\quad +k_0^4\left[\varsigma_{xx}^{(1)}\varsigma_{yy}^{(1)}\varsigma_{zz}^{(1)} - \varsigma_{yy}^{(1)}\varsigma_{zx}^{(1)}\varsigma_{xz}^{(1)} + \varsigma_{xy}^{(1)}\left(\varsigma_{yz}^{(1)}\varsigma_{zx}^{(1)} - \varsigma_{zz}^{(1)}\varsigma_{yx}^{(1)}\right)\right.\\
&\quad \left.+\varsigma_{zy}^{(1)}\left(\varsigma_{xz}^{(1)}\varsigma_{yx}^{(1)} - \varsigma_{yz}^{(1)}\varsigma_{xx}^{(1)}\right)\right].
\end{aligned} \tag{17}$$

The dispersion relation for *bulk* polaritons is then obtained straightforwardly from (16) by putting $\kappa = 0$ inside it.

In order to find the dispersion law of surface polaritons from four roots of (16), two physically correct ones must be selected. In general, two such roots are required to satisfy the electromagnetic boundary conditions at the surface of the composite medium. We define these roots as κ_1 and κ_2 and then following [10] introduce the quantities K_w ($w = 1, 2$) in the form:

$$\begin{aligned}
P_x^{(1)}(\kappa_w) &= K_w A_{zx}(\kappa_w),\\
P_y^{(1)}(\kappa_w) &= K_w C(\kappa_w),\\
P_z^{(1)}(\kappa_w) &= -K_w B_{zx}(\kappa_w),
\end{aligned} \tag{18}$$

where $C(\kappa_w) = -\left(1/\varkappa_y^2\right)\left[\left(ik_x\kappa_w - k_0^2\varsigma_{yx}^{(1)}\right)A_{zx}(\kappa_w) + \left(ik_z\kappa_w - k_0^2\varsigma_{yz}^{(1)}\right)B_{zx}(\kappa_w)\right]$.

In (18), unknown quantities K_w need to be determined from the boundary conditions.

http://dx.doi.org/10.5772/intechopen.71837

Taking into consideration that two appropriate roots κ_1 and κ_2 of (16) are selected, the components of the field $\vec{P}^{(1)}$ can be rewritten as the linear superposition of two terms:

$$\begin{aligned} P_x^{(1)} &= \sum_{w=1,2} K_w A_{zx}(\kappa_w) \exp(\kappa_w y), \\ P_y^{(1)} &= \sum_{w=1,2} K_w C(\kappa_w) \exp(\kappa_w y), \\ P_z^{(1)} &= \sum_{w=1,2} K_w B_{zx}(\kappa_w) \exp(\kappa_w y), \end{aligned} \tag{19}$$

where $y < 0$ and the factor $\exp[i(k_x x + k_z z - \omega t)]$ is omitted.

Involving a pair of the divergent Maxwell's equations $\nabla \cdot \vec{B} = 0$ and $\nabla \cdot \vec{D} = 0$ in the form

$$\nabla \cdot \vec{Q}^{(j)} = \nabla \cdot \left(\hat{g}^{(j)} P^{(j)} \right) = 0, \tag{20}$$

where g is substituted for permeability μ and permittivity ε and $\vec{Q}$ is substituted for the magnetic $\vec{B}$ and electric $\vec{D}$ flux densities; one can immediately obtain the relations between the field components in the upper ($y > 0$) medium as follows:

$$Q_y^{(0)} = \left(i g_0 / \kappa_0 \right) \left(k_x P_x^{(0)} + k_z P_z^{(0)} \right). \tag{21}$$

The boundary conditions at the interface require the continuity of the tangential components of $\vec{E}$ and $\vec{H}$ as well as the normal components of $\vec{D}$ and $\vec{B}$, i.e., in our notations these components are P_x, P_z, and Q_y, respectively. Thus, application of the boundary conditions together with (21) gives us the next set of equations:

$$\begin{aligned} &\left(i g_0 / \kappa_0 \right) \left(k_x P_x^{(0)} + k_z P_z^{(0)} \right) = \tilde{g}_{yx} \sum_{w=1,2} K_w A_{zx}(\kappa_w) \\ &\quad + \tilde{g}_{yx} \sum_{w=1,2} K_w C(\kappa_w) - \tilde{g}_{yz} \sum_{w=1,2} K_w B_{zx}(\kappa_w), \\ &P_x^{(0)} = \sum_{w=1,2} K_w A_{zx}(\kappa_w), \\ &P_z^{(0)} = - \sum_{w=1,2} K_w B_{zx}(\kappa_w), \\ &k_z P_x^{(0)} - k_x P_z^{(0)} = k_z \sum_{w=1,2} K_w A_{zx}(\kappa_w) + k_x \sum_{w=1,2} K_w B_{zx}(\kappa_w). \end{aligned} \tag{22}$$

The system of Eq. (22) has a nontrivial solution only if its determinant vanishes. Applying this condition gives us the required dispersion equation for *surface* polaritons.

Finally, the amplitudes K_1 and K_2 can be found by solving set of linear homogeneous Eq. (22). They are

$$\begin{aligned} K_1 &= [k_x A_{zx}(\kappa_2) + k_z B_{zx}(\kappa_2)](\kappa_0 + \kappa_2), \\ K_2 &= -[k_x B_{zx}(\kappa_1) + k_z A_{zx}(\kappa_1)](\kappa_0 + \kappa_1). \end{aligned} \tag{23}$$

Here, the problem is considered to be formally solved, and the dispersion relations are derived in a general form for both bulk and surface polaritons.

4. Theory of Morse critical points: mode coupling phenomena

Further, for brevity, obtained dispersion equations for the bulk and surface polaritons are denoted in the form:

$$\mathfrak{D}(k, k_0) = 0. \tag{24}$$

Numerical solution of Eq. (24) gives a set of dispersion curves $k_0(k)$ of polaritons, which can contain both regular and singular (critical) points. The regular points draw dispersion curves of a classical form possessing either normal or anomalous dispersion line, at which a small variation in k_0 results in a smooth changing in the form of the curves. Besides, some situations are possible when a slight variation in k_0 leads to a very sharp (catastrophic) changing in the form of dispersion curves. Such singularities (extreme states) can be accompanied by mutual coupling phenomena of modes, which are further of our interest.

From the mathematical point of view the found extreme states in dispersion curves exist in the region where the differential $\mathfrak{D}'(k, k_0)$ of dispersion Eq. (24) vanishes (see, e.g., **Figure 3**). These extreme states can be carefully identified and studied involving the approach based on the theory of the Morse critical points from the catastrophe theory [31–36]. This treatment has been originally applied to study open waveguides and resonators [31, 32], and later it has been extended to more complex waveguide structures [33–35]. From viewpoint of this theory, the presence of the Morse critical points is generally defined by a set of nonlinear differential equations written in the form [33]:

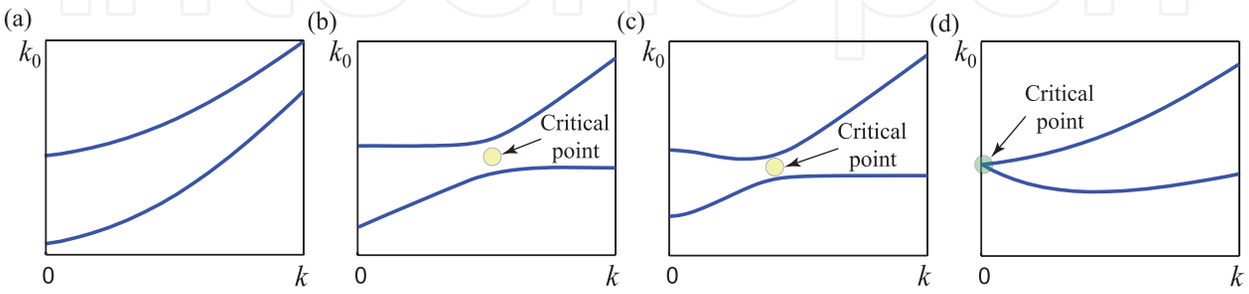

Figure 3. Sketch of the band diagrams presenting different kinds of interaction between two neighboring modes: (a) weak interaction, (b) intermediate interaction, (c) strong interaction, and (d) accidental degeneracy. Areas where the critical points exist are pointed by circles.

http://dx.doi.org/10.5772/intechopen.71837

$$\begin{gathered}\mathfrak{D}'_k(k,k_0)\big|_{\left(k^m,k_0^m\right)} = \mathfrak{D}'_{k_0}(k,k_0)\big|_{\left(k^m,k_0^m\right)} = 0,\\ \mathbb{H} = [h_{11}h_{22} - h_{12}h_{21}]\big|_{\left(k^m,k_0^m\right)} \neq 0,\end{gathered} \tag{25}$$

where $\left(k^m, k_0^m\right)$ are coordinates in the $k - k_0$ plane of a particular m-th Morse critical point, the subscripts k and k_0 near the letter $\mathfrak{D}$ define corresponding partial derivatives $\partial/\partial k$ and $\partial/\partial k_0$, and $\mathbb{H}$ is the Hessian determinant with elements:

$$\begin{aligned} h_{11} &= \mathfrak{D}''_{kk}(k,k_0), \quad h_{12} = \mathfrak{D}''_{kk_0}(k,k_0),\\ h_{21} &= \mathfrak{D}''_{k_0k}(k,k_0), \quad h_{22} = \mathfrak{D}''_{k_0k_0}(k,k_0).\end{aligned} \tag{26}$$

The type of each extreme state defined by set of Eq. (25) can be uniquely identified from the sign of the Hessian determinant [35]. For instance, when $\mathbb{H} < 0$, the corresponding Morse critical point represents a saddle point, which occurs in the region of a modal coupling (the *anti-crossing* effect), whereas in the case of degeneracy, when $\mathbb{H} = 0$, it is a non-isolated critical point (the *crossing* effect). In the case when $\mathbb{H} > 0$, the Morse critical point defines either a local minimum or maximum (this case is not considered here). In what follows we distinguish found critical points by circles for both crossing and anti-crossing effects, as shown in **Figure 3**.

In general, when conditions (25) are met, the type of interacting modes in the vicinity of the corresponding Morse critical point can be defined as follows [33]:

$$\textit{Codirectional forward}: \quad h_{12}/h_{11} < 0, \quad h_{22}/h_{11} > 0; \tag{27}$$

$$\textit{Codirectional backward}: \quad h_{12}/h_{11} > 0, \quad h_{22}/h_{11} > 0; \tag{28}$$

$$\textit{Contradirectional}: \quad h_{12}/h_{11} > 0, \quad h_{22}/h_{11} < 0. \tag{29}$$

The strength of modes interaction within the found extreme states in the region of their coupling can be identified considering the classification introduced in paper [37], which concerns on the mode behaviors appearing in axial waveguides. In particular, (i) a weak interaction takes place when frequency band gap between dispersion curves of interacting modes is high enough (**Figure 3a**), (ii) an intermediate interaction of modes leads to formation of very flattened parts in the dispersion curves (**Figure 3b**), (iii) a strong interaction appears when the repulsion between modes is strong enough resulting in formation of dispersion curve having anomalous dispersion line (**Figure 3c**), and (iv) an accidental degeneracy arises when two dispersion branches are merged within the critical point which leads to nonzero group velocities at $k = 0$ (**Figure 3d**).

The strong interaction with forming negative-slope region in dispersion curve of one of interacting modes (as it is depicted in **Figure 3c** and **d**) leads to some unusual effects [37]. First, zero group velocity ($v_g = \partial k_0/\partial k$) can appear at a nonzero value of k. The flattened region of the dispersion curve around that extreme point (**Figure 3c**) is very useful for applications in nonlinear optics, where a small group velocity is suitable for enhancing nonlinear effects, while the phase-matching criterion can still be satisfied because the wave vector is nonzero. Second,

when interacting modes are exactly degenerated, then their group velocities appear to be nonzero and roughly constant values as $k \to 0$ (**Figure 3d**). From viewpoint of practical applications, this situation is useful, because regular modes in the vicinity of $k = 0$ have extremely small value of their group velocity and thus become unusable. Since both dispersion and losses are inversely proportional to $v_{g,}$ they diverge when $k \to 0$.

At the same time, the intermediate interaction with forming extremely flattened part in the mode dispersion curve (see **Figure 3b**) leads to strong divergence in density of states, and it can be utilized in designs of low-threshold lasers [37].

5. Dispersion features of bulk and surface polaritons for three particular orientations of magnetization

Since further our goal is to elucidate the dispersion laws of the bulk and surface polaritons (which are in fact *eigenwaves*), we are interested in real solutions of Eq. (24). In order to find the real solutions, the absence of losses in constitutive parameters of the underlying layers is supposed.

We consider three particular orientations of the external magnetic field $\vec{M}$ with respect to the superlattice's interface (the $x - z$ plane) and to the wave vector $\vec{k}$, namely, (i) the *polar geometry* in which the external magnetic field is applied perpendicular to both the direction of wave propagation ($\vec{M} \perp \vec{k}$) and structure's interface ($\vec{M} \| y$) as shown in **Figure 4a**; (ii) the *Voigt geometry* in which the external magnetic field is applied parallel to the structure's interface, and it is perpendicular to the direction of the wave propagation, so $\vec{M} \| z$ and $\vec{M} \perp \vec{k}$ as presented in **Figure 4b**; (iii) the *Faraday geometry* in which the external magnetic field is applied parallel to both the direction of wave propagation and structure's interface, i.e., $\vec{M} \| z$ and $\vec{M} \| \vec{k}$ as presented in **Figure 4c**.

With respect to the problem of polaritons, in any kind of an unbounded gyrotropic medium, there are two distinct eigenwaves (the bulk waves), whereas the surface waves split apart only

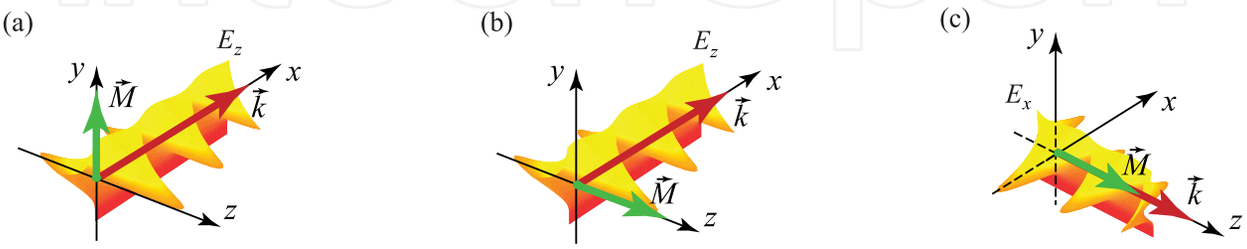

Figure 4. Three particular orientations of the external magnetic field vector $\vec{M}$ with respect to the superlattice's interface and wave vector; (a) polar geometry, $\vec{M} \| y$, $\vec{M} \perp \vec{k}$; (b) Voigt geometry, $\vec{M} \| z$, $\vec{M} \perp \vec{k}$; and (c) Faraday geometry $\vec{M} \| z$, $\vec{M} \| \vec{k}$.

http://dx.doi.org/10.5772/intechopen.71837

for some particular configurations (e.g., for the Voigt geometry), and generally, the field has all six components. Such surface waves are classified as hybrid EH modes and HE modes, and these modes appear as some superposition of longitudinal and transverse waves. By analogy with [38], we classify hybrid modes depending on the magnitude ratio between the longitudinal electric and magnetic field components (P_x and P_z components for the polar and Faraday geometries, respectively). For instance, for the polar configuration, it is supposed that the wave has the EH type if $E_x > H_x$ and the HE type if $H_x > E_x$. Contrariwise, in the Faraday geometry, we stipulate that the wave has the EH type if $E_z > H_z$ and the HE type if $H_z > E_z$. In the Voigt geometry, the waves appear as transverse electric (TE) and transverse magnetic (TM) modes, where each of them has three field components.

The polariton dispersion relations for these specific cases of magnetization can be obtained using general results derived in Section 3 with application of appropriate boundary and initial conditions.

When an external static magnetic field is influenced in the Voigt geometry ($\vec{M} \| z, \quad \vec{M} \perp \vec{k}$), solution of Eq. (16) for both bulk and surface waves splits apart into two independent equations for distinct polarizations [10], namely, TE modes with field components $\{H_x, H_y, E_z\}$ and TM modes with field components $\{E_x, E_y, H_z\}$. Therefore, regions of existence of bulk polaritons are uniquely determined by solutions of two separated equations related to the TE and the TM modes as follows [26, 38]:

$$k_x^2 - k_0^2 \varepsilon_{zz} \mu_v \mu_{yy} \mu_{xx}^{-1} = 0, \tag{30}$$

$$k_x^2 - k_0^2 \mu_{zz} \varepsilon_v \varepsilon_{yy} \varepsilon_{xx}^{-1} = 0, \tag{31}$$

where $\varepsilon_v = \varepsilon_{xx} + \varepsilon_{xy}^2/\varepsilon_{yy}$ and $\mu_v = \mu_{xx} + \mu_{xy}^2/\mu_{yy}$ are the Voigt relative permittivity and permeability, respectively.

Under such magnetization, the dispersion equation for the surface polaritons at the interface between vacuum and the given structure has the form [26]:

$$\kappa_1 g_v + \kappa_2 g_0 + i k_x g_0 \tilde{g}_{xy} \tilde{g}_{yy}^{-1} = 0, \tag{32}$$

where substitutions $\mu \to g$ and $\varepsilon \to g$ are related to the TE and TM modes, respectively.

We should note that in two particular cases of the gyroelectric and gyromagnetic superlattices, dispersion relation (32) coincides with Eq. (33) of Ref. [10] and Eq. (21) of Ref. [15], respectively, which verifies the obtained solution.

It follows from **Figure 4b** that in the Voigt geometry, the magnetic field vector in the TM mode has components $\{0, 0, H_z\}$, and it is parallel to the external magnetic field $\vec{M}$, which results in the absence of its interaction with the magnetic subsystem [39–41]. Thus, hereinafter dispersion features only of the TE mode are of interest for which the dispersion equation for surface polaritons (32) can be rewritten as

$$\kappa_1 \mu_v + \kappa_2 \mu_0 + i k_x \mu_0 \mu_{xy} \mu_{yy}^{-1} = 0. \tag{33}$$

Importantly, since the dispersion equation consists of a term which is linearly depended on k_x (the last term in (33)), the spectral characteristics of the surface polaritons in the structure under study possess the nonreciprocal nature, i.e., $k_0(k_x) \neq k_0(-k_x)$.

A complete set of dispersion curves obtained from solution of Eq. (30) that outlines the passbands of the TE bulk polaritons as a function of the filling factor δ_m is presented in **Figure 5a**. One can see that behaviors of the TE bulk polaritons are quite trivial in the overwhelming majority of structure's configurations, namely, there are two isolated passbands separated by a forbidden band. The upper passband is bounded laterally by the light line, and its lower limit is restricted by the line at which $\mu_v = 0$. The bottom passband starts on the line where $\varepsilon_{zz} = 0$ and then approaches the asymptotic frequency ($k_x \to \infty$) at which $\mu_{xx} = 0$ (see Eq. (25)).

In this study, we are mainly interested in those curves of the set which have greatly sloping branches and exhibit the closest approaching each other (i.e., they manifest the anti-crossing effect) or have a crossing point, since such dispersion behaviors correspond to the existence of the Morse critical points. Hereinafter, the areas of interest in which these extreme states exist are denoted in figures by orange circles.

It follows from **Figure 5a** that in the Voigt geometry, both the anti-crossing ($\mathbb{H} < 0$) and crossing ($\mathbb{H} = 0$) effects with forming the bottom branch characterized by the anomalous dispersion (i.e., the strong mode interaction occurs) can be achieved in the composite structure with a predominant impact of the semiconductor subsystem (further we stipulate that the composite system has a predominant impact of either magnetic subsystem or semiconductor subsystem if $\delta_m \gg \delta_s$ or $\delta_s \gg \delta_m$, respectively). Moreover, since condition (29) is met near the critical point, the bulk waves appear to be contradirectional.

The crossing effect is found to be at $k_x \to 0$ (accidentally degenerate modes) for the particular configuration of the structure, when $\delta_m = 0.132$ (**Figure 5b**). Remarkably, such an extreme state corresponds to a particular frequency where ε_{zz} and μ_v simultaneously acquire zero [26].

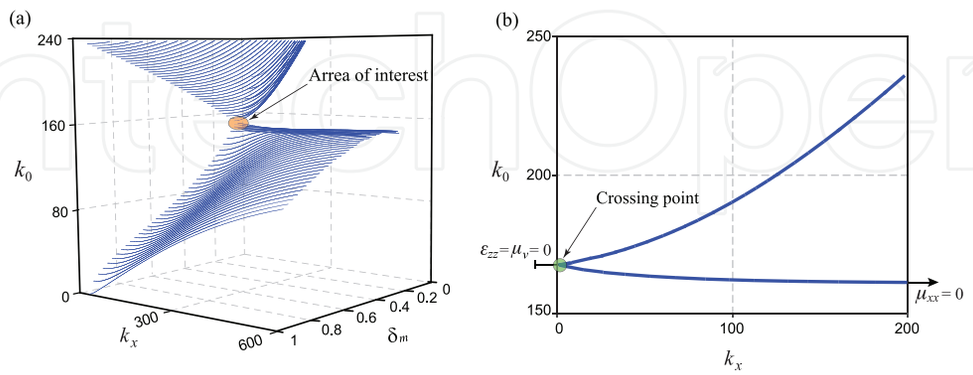

Figure 5. (a) A set of dispersion curves of the TE bulk polaritons for different filling factors δ_m for the structure being in the Voigt geometry and (b) manifestation of crossing effect in dispersion curves of the TE bulk polaritons at the particular value of filling factor $\delta_m = 0.132$. Parameters of magnetic constitutive layers are shown in **Figure 2**. For the semiconductor constitutive layers, parameters are $f_p = \omega_p/2\pi = 10.5$ GHz, $f_c = \omega_c/2\pi = 9.5$ GHz, $\nu = 0$, $\varepsilon_l = 1.0$, and $\mu_s = 1.0$.

http://dx.doi.org/10.5772/intechopen.71837

In the polar geometry ($\vec{M} \| y, \quad \vec{M} \perp \vec{k}$), composite medium under study is a uniaxial crystal whose optical axis is directed along the y-axis. In this case, bulk polaritons split onto two waves with field components $\{E_x, H_y, E_z\}$ and $\{H_x, E_y, H_z\}$, respectively [40], and their continua is outlined by two dispersion relations:

$$k_x^2 - k_0^2 \mu_{yy} \varepsilon_{yy} = 0, \tag{34}$$

$$k_x^2 - k_0^2 \mu_v \varepsilon_v \left[1 - \mu_{xz} \varepsilon_{xz} / \left(\mu_{xx} \varepsilon_{xx}\right)\right]^{-1} = 0, \tag{35}$$

where $\varepsilon_v = \varepsilon_{xx} + \varepsilon_{xz}^2 / \varepsilon_{xx}$ and $\mu_v = \mu_{xx} + \mu_{xz}^2 / \mu_{xx}$ are introduced as the effective bulk permeability and permittivity, respectively.

Hereinafter, we distinguish these two kinds of waves as ordinary and extraordinary bulk polaritons, respectively (note: such a definition is common in the plasma physics [43]).

In order to elucidate the dispersion features of hybrid surface polaritons, the initial problem is decomposed into two particular solutions with respect to the vector $\vec{H}$ (EH modes) and vector $\vec{E}$ (HE modes) [10, 42]. In this way, the dispersion equation for surface polaritons is derived in the form:

$$\begin{aligned} &\kappa_0^2 \tilde{g}_{xx} g_0^{-1} \left[\left(\kappa_1^2 + \kappa_1 \kappa_2 + \kappa_2^2 - \varkappa_z^2\right) + \varkappa_y^2 \varsigma_{xz} \tilde{g}_{xz} \left(\varsigma_{yy} \tilde{g}_{xx}\right)^{-1}\right] \\ &+ \kappa_0 (\kappa_1 + \kappa_2) \left[\kappa_1 \kappa_2 + \varkappa_y^2 \tilde{g}_{xx} g_v \left(g_0 \varsigma_{yy}\right)^{-1}\right] \\ &+ \tilde{g}_{xz} \varsigma_{xz}^{-1} \left[\left(\varkappa_z^4 - \varkappa_z^2 (\kappa_1 + \kappa_2) + \kappa_1^2 \kappa_2^2\right) + \varkappa_y^2 \left(\varkappa_z^2 + \kappa_1 \kappa_2\right) \varsigma_{xz} \tilde{g}_{zz} \left(\varsigma_{yy} \tilde{g}_{xz}\right)^{-1}\right] = 0, \end{aligned} \tag{36}$$

where $\varkappa_v^2 = k_x^2 - k_0^2 \varsigma_{vv}$ and two distinct substitutions $\varepsilon_{vv'} \to \tilde{g}_{vv'}$, $\varepsilon_0 \to g_0$, $\varepsilon_v \to g_v$ and $\varepsilon_{vv'} \to \tilde{g}_{vv'}$, $\mu_0 \to g_0$, $\mu_v \to g_v$ correspond to the problem resolving with respect to the vector $\vec{E}$ and vector $\vec{H}$, respectively; ε_v and μ_v are the same shown in Eqs. (34) and (35).

For two particular cases of the gyroelectric and gyromagnetic superlattices, dispersion relation (36) coincides with Eq. (23) of Ref. [10] and Eq. (21) of Ref. [13], respectively, which verifies the obtained solution.

Complete sets of dispersion curves calculated from the solution of Eqs. (34) and (35) that outline the passbands of both ordinary (blue curves) and extraordinary (red curves) bulk polaritons as functions of the filling factor δ_m are presented in **Figure 6a** and **b**. Moreover, in order to discuss the observed crossing and anti-crossing effects more clearly, dispersion curves of both ordinary and extraordinary bulk polaritons are plotted in the $k_0 - k_x$ plane at the particular values of filling factor δ_m as shown in **Figure 6c–f**.

From **Figure 6a** one can conclude that there are two isolated areas of existence of the ordinary bulk polaritons. The upper passband starts at the frequency where $\varepsilon_{yy} = 0$, while the bottom passband is bounded above by the asymptotic line where $\varepsilon_{yy} \to \infty$. Remarkably, the anti-

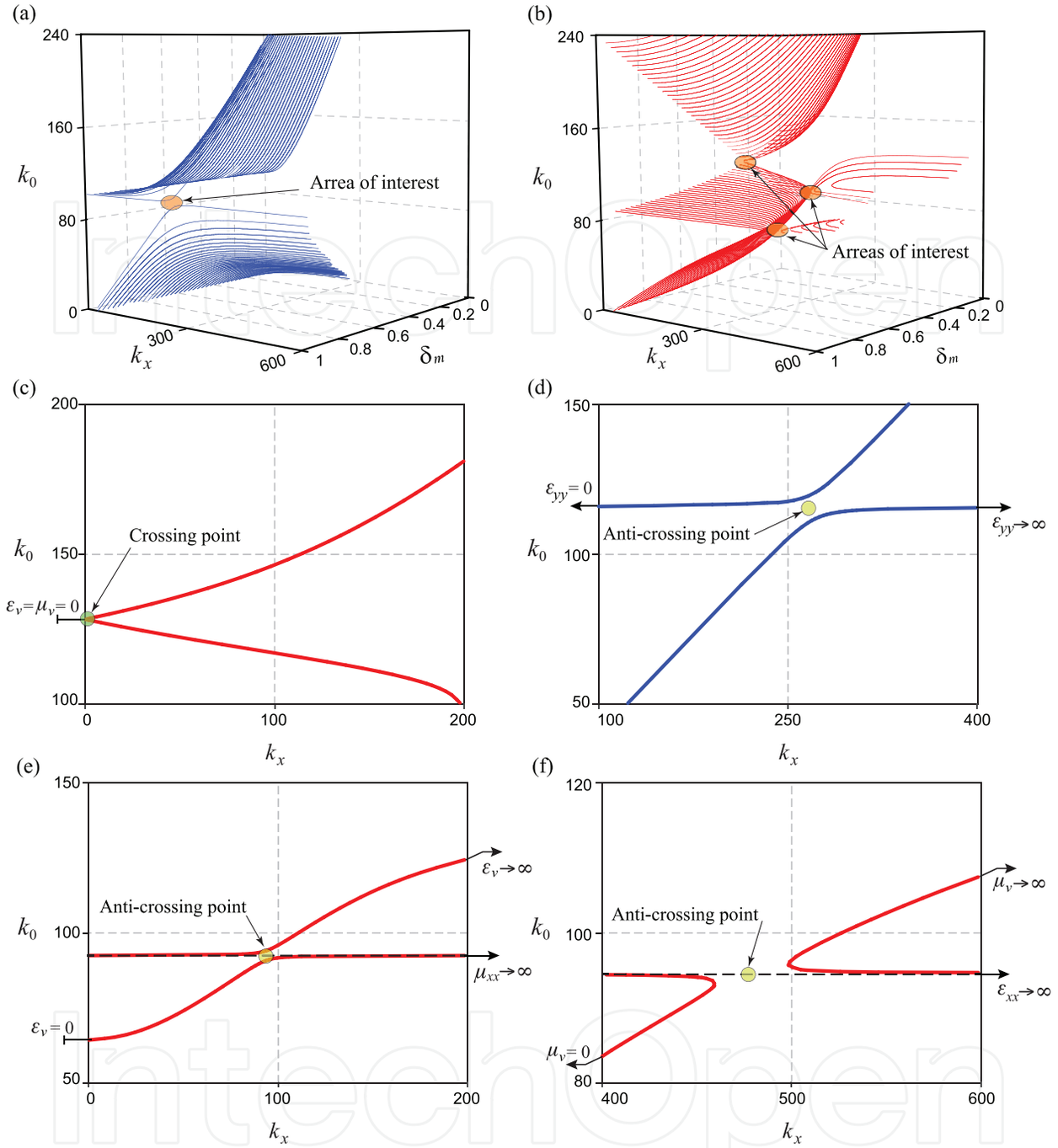

Figure 6. Complete sets of dispersion curves of (a) ordinary (blue curves) and (b) extraordinary (red curves) bulk polaritons for different filling factor δ_m for the structure being in the polar geometry. Manifestation of (c) crossing and (d–f) anti-crossing effects in dispersion curves of bulk polaritons at the particular value of filling factor δ_m, (c) $\delta_m = 0.267$, (d) $\delta_m = 0.99$, (e) $\delta_m = 0.05$, and (f) $\delta_m = 0.99$. All structure constitutive parameters are shown in **Figure 2**.

crossing effect ($\mathbb{H} < 0$) between dispersion curves which restrict upper and bottom passbands of ordinary bulk polaritons can be observed in the composite structure with a predominant impact of the magnetic subsystem (i.e., $\delta_m \gg \delta_s$) as presented in **Figure 6a** and **d**. Coupled modes exhibit an intermediate interaction for which an appearance of the flattened branches in

dispersion curves is peculiar (see, for instance, **Figure 3b**). Besides, condition (27) is met, so these waves are codirectional forward in the area nearly the critical point.

As shown in **Figure 6b**, there are two separated areas of existence of extraordinary bulk polaritons for each particular filling factor δ_m. Moreover, there are two possible combinations of conditions for their passbands, which depend strictly on the value of filling factor δ_m [42]. Therefore, the particular critical filling factor is denoted here as δ_c at which $\varepsilon_v = \mu_v = 0$ at $k_x = 0$, and it is considered as a separation point between these two combinations. Thus, the overall range of values δ_m can be separated onto two subranges $0 \le \delta_m < \delta_c$ and $\delta_c < \delta_m \le 1$, respectively.

The value of the critical filling factor δ_c depends on the constitutive parameters of magnetic and semiconductor layers, and for the structure under study, it is $\delta_c = 0.267$. Such critical state in the effective parameters of the superlattice leads to the absence of the forbidden band between the upper and bottom passbands as shown in **Figure 6c**. Remarkably, these dispersion branches appear to be coupled exactly at the frequency where $\varepsilon_v = \mu_v = 0$, i.e., the crossing effect ($\mathbb{H} = 0$) is found to be at $k_x \to 0$. Besides, such coupled waves are contradirectional, and they are described by condition (29).

At the same time, for all present values of filling factor δ_m from the first subrange $0 \le \delta_m < \delta_c$, the lower limits of both the upper and bottom passbands are restricted by the lines at which $\varepsilon_v = 0$, as well as the bottom passband is bounded above by the asymptotic line where $\varepsilon_v \to \infty$. The upper passband is outlined by the set of following conditions [40]: $\varepsilon_v > 0$, $\mu_v > 0$, $\varepsilon_{xz}\mu_{xz}/\varepsilon_{xx}\mu_{xx} < 1$. The bottom passband exists when the set of following conditions holds [42]: $\varepsilon_v > 0$, $\mu_v < 0$ and $\varepsilon_{xz}\mu_{xz}/\varepsilon_{xx}\mu_{xx} > 1$ or $\varepsilon_v > 0$, $\mu_v > 0$ and $\varepsilon_{xz}\mu_{xz}/\varepsilon_{xx}\mu_{xx} < 1$.

For all other values of filling factor δ_m (i.e., $\delta_c < \delta_m \le 1$), the conditions for the upper passband are the same (i.e., $\varepsilon_v > 0$, $\mu_v > 0$, $\varepsilon_{xz}\mu_{xz}/\varepsilon_{xx}\mu_{xx} < 1$), whereas its lower limit is at the line where $\mu_v = 0$. The bottom passband exists when either the set of conditions $\varepsilon_v < 0$, $\mu_v > 0$ and $\varepsilon_{xz}\mu_{xz}/\varepsilon_{xx}\mu_{xx} > 1$ or $\varepsilon_v > 0$, $\mu_v > 0$ and $\varepsilon_{xz}\mu_{xz}/\varepsilon_{xx}\mu_{xx} < 1$ is satisfied. For this band, the lower and upper limits are restricted by the lines at which $\mu_v = 0$ and $\mu_v \to \infty$, respectively.

From **Figure 6a** and **b**, one can conclude that the upper passband possesses typical behaviors in the $k_0 - k_x$ plane, whereas the width and position of the bottom passbands are defined by the corresponding resonant frequencies of effective bulk permeability μ_v and effective bulk permittivity ε_v. In fact, these constitutive parameters are multipliers of the numerator of Eq. (35), whereas the denominator of this equation originates a singularity at the asymptotic line where $1 - \varepsilon_{xz}\mu_{xz}/\varepsilon_{xx}\mu_{xx} \to \infty$. This asymptotic line splits the bottom passbands onto two separated sub-passbands which corresponds to the structures with a predominant impact of semiconductor and magnetic subsystems, respectively (**Figure 6e** and **f**). Note, the intermediate interaction with forming flattened region in dispersion curves between bulk modes from these two sub-bands is observed nearly the Morse critical points ($\mathbb{H} < 0$). Such coupled waves are contradirectional since condition (29) is met.

In the Faraday geometry ($\vec{M} \| z$, $\vec{M} \| \vec{k}$), the superlattice is characterized by the biaxial anisotropy, for which, as already mentioned, the first anisotropy axis is associated with the structure

periodicity (so it is directed along the y-axis), while the second anisotropy axis is a result of the external static magnetic field influence (so it is directed along the z-axis). For this geometry, the bulk polaritons in the structure under study appear as right-handed and left-handed elliptically polarized waves [10, 12, 44], and their passbands are outlined by curves governed by the following dispersion law [44]:

$$\varkappa_x^2\varkappa_y^2 - k_0^4\varsigma_{xy}\varsigma_{yx} = 0, \tag{37}$$

where $\varkappa_\nu^2 = k_z^2 - k_0^2\varsigma_{\nu\nu}$.

The surface polaritons are hybrid EH and HE waves, and their dispersion relation can be written in the form [44]:

$$\begin{aligned}&\left(\kappa_2 + \kappa_0\tilde{g}_{zz}\right)\left(\kappa_2^2\varsigma_{yy} - \varkappa_y^2\varsigma_{zz}\right)\left\{\kappa_1\psi\left(\kappa_0^2 - k_z^2\right) + \kappa_0\left[\kappa_1^2\tilde{g}_{xy}\varsigma_{yy} - \varsigma_{zz}\left(k_0^2\rho + k_z^2\tilde{g}_{xy}\right)\right]\right\}\\ &-\left(\kappa_1 + \kappa_0\tilde{g}_{zz}\right)\left(\kappa_1^2\varsigma_{yy} - \varkappa_y^2\varsigma_{zz}\right)\left\{\kappa_2\psi\left(\kappa_0^2 - k_z^2\right) + \kappa_0\left[\kappa_2^2\tilde{g}_{xy}\varsigma_{yy} - \varsigma_{zz}\left(k_0^2\rho + k_z^2\tilde{g}_{xy}\right)\right]\right\} = 0.\end{aligned} \tag{38}$$

In Eq. (38), two distinct substitutions $\varepsilon_{vv'} \to \tilde{g}_{vv'}$, $\varepsilon_v \to g_v$ and $\mu_{vv'} \to \tilde{g}_{vv'}$, $\mu_v \to g_v$ correspond to the problem resolving with respect to the vector $\vec{E}$ and vector $\vec{H}$, respectively; $\varepsilon_v = \varepsilon_{xx} + \varepsilon_{xy}^2/\varepsilon_{yy}$, $\mu_v = \mu_{xx} + \mu_{xy}^2/\mu_{yy}$, $\psi = g_v\tilde{g}_{yy}\varsigma_{yx}$; $\rho = \tilde{g}_{yy}\varsigma_{yx} - \tilde{g}_{xy}\varsigma_{yy}$; and the constant $g_0 = 1$ is omitted.

For the semiconductor superlattice, the dispersion Eq. (38) agrees with Eq. (38) of Ref. [10], while in the case of magnetic superlattice, it coincides with Eq. (13) of Ref. [12], which verifies the obtained solution.

Complete sets of dispersion curves that outline the bands of existence of the bulk polaritons (see Eq. (37)) as functions of filling factor δ_m are presented in **Figure 7a** and **b** for right-handed (blue curves) and left-handed (red curves) elliptical polarizations. From these figures, one can conclude that there is a pair of corresponding sets of dispersion curves separated by a forbidden band for the bulk polaritons of each polarization. The dispersion curves of the right-handed elliptically polarized bulk waves demonstrate quite trivial behaviors, and they completely inherit characteristics of the right-handed circularly polarized waves of the corresponding reference semiconductor or magnetic medium (see, for instance [44]). Contrariwise, the dispersion features of the left-handed elliptically polarized waves are much more complicated being strongly dependent on filling factor δ_m and resonant frequencies of constitutive parameters of both semiconductor and magnetic underlying materials. Therefore, in what follows we are interested only in the consideration of dispersion features of the bulk polaritons having the left-handed polarization.

One can conclude that the dispersion characteristics of the left-handed elliptically polarized bulk waves of the given gyroelectromagnetic structure are different from those ones of both convenient gyroelectric and gyromagnetic media. Indeed, in contrast to the characteristics of the left-handed circularly polarized waves of the corresponding reference medium whose passband has no discontinuity, the passband of the left-handed elliptically polarized bulk

http://dx.doi.org/10.5772/intechopen.71837

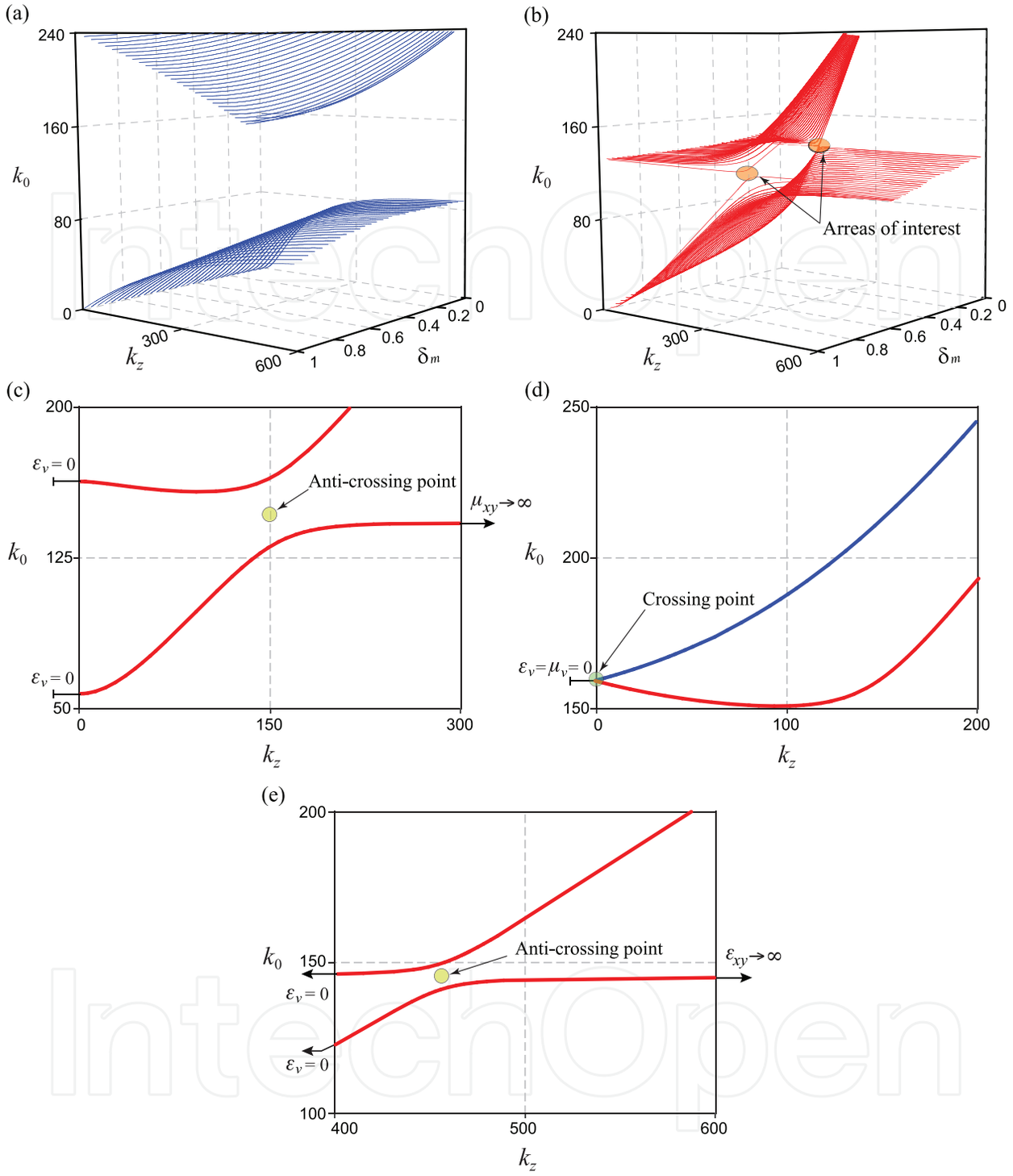

Figure 7. (a, b) Complete sets of dispersion curves of both right-handed (blue curves) and left-handed (red curves) elliptically polarized bulk polaritons for different filling factor δ_m for the structure being in the Faraday geometry. Manifestation of (c, e) anti-crossing and (d) crossing effects in dispersion curves of bulk polaritons at the particular value of filling factor δ_m; (c) $\delta_m = 0.15$; (d) $\delta_m = 0.1$; and (e) $\delta_m = 0.95$. All structure constitutive parameters are shown in **Figure 2**.

polaritons of the superlattice is separated into two distinct areas. This separation appears nearly the frequency at which the resonances of the functions ε_{xy} and μ_{xy} occur for the composite structures with predominant impact of the magnetic and semiconductor subsystems,

respectively. Also, we should note that the exchange by the critical conditions for the asymptotic lines (at which $k_z \to \infty$) between the bottom passbands of left-handed and right-handed elliptically polarized bulk polaritons appears at the particular frequency where ε_{xy} and μ_{xy} simultaneously tend to infinity.

The dispersion curves of bulk waves, which have left-handed polarization, demonstrate significant variation of their slope having subsequent branches with normal and anomalous dispersion that possess approaching at some points (extreme states) as depicted in **Figure 7c** and **e**. The features of these dispersion curves in the vicinity of the critical points are different for the composite structure which has predominant impact either semiconductor (i.e., $\delta_s \gg \delta_m$) or magnetic (i.e., $\delta_m \gg \delta_s$) subsystem. The corresponding modes are contradirectional (i.e., condition (29) is met), and they demonstrate strong interaction nearly the Morse critical point (the anti-crossing effect with $\mathbb{H} < 0$) in the case when $\delta_s \gg \delta_m$. The modes acquire an intermediate interaction in the superlattice with predominant impact of the magnetic subsystem as depicted in **Figure 7e**.

Moreover, a particular extreme state in dispersion curves is found out where the upper branches of the left-handed and right-handed elliptically polarized bulk polaritons merge with each other (see **Figure 6d**) and crossing point ($\mathbb{H} = 0$) occurs at $k_z \to 0$. Likewise to the polar geometry, such extreme state corresponds to the particular superlattice configuration where $\varepsilon_v = \mu_v = 0$ at $k_z = 0$. So, the interacting waves are degenerated at this point and possess the contradirectional propagation.

We should note that in [37] some unusual and counterintuitive consequences of such behaviors of the dispersion curves (e.g., backward wave propagation, reversed Doppler shift, reversed Cherenkov radiation, atypical singularities in the density of states, etc.) for the TE and TM modes of an axially uniform waveguide are discussed, and it is emphasized that these effects are of considerable significance for practical applications.

Finally, in order to obtain the dispersion curves $k_0(k)$ of surface polaritons in both the polar and Faraday configurations, characteristic Eqs. (36) and (38) are solved numerically [42, 44]. Here, as previously, the problem is decomposed into two particular solutions with respect to the vector $\vec{H}$ (EH waves) and vector $\vec{E}$ (HE waves) [10, 12]. Note, as evident from Eqs. (36) and (38), k_x and k_z appear only in even powers, so the dispersion curves of the surface waves appear to be reciprocal.

For both initial problem considerations, dispersion Eqs. (36) and (38) have four roots from which two physically correct ones (denoted here as κ_1 and κ_2) are selected [10] ensuring they correspond to the attenuating waves. In papers [10] and [12], it was noted that depending upon the position in the $k_0 - k_w$ plane, in the non-dissipative system, the following combinations between two roots κ_1 and κ_2 may arise: (i) both roots are real and positive (bona fide surface modes); (ii) one root is real and the other is pure imaginary or vice versa (pseudosurface modes); (iii) both roots are complex in which case they are conjugate (generalized surface modes); and (iv) both roots are pure imaginary (the propagation is forbidden). In our study we consider only bona fide surface mode. Nevertheless, we should note that in both

http://dx.doi.org/10.5772/intechopen.71837

the polar and Faraday geometries, pseudosurface waves (which attenuate only on one side of the surface) can also be supported [10, 45].

Among all possible appearance of dispersion curves of the surface polaritons, we are only interested in those ones which manifest the crossing or anti-crossing effect. The search of their existence implies solving an optimization problem, where for the crossing effect the degeneracy point should be found. For the anti-crossing effect, the critical points are defined from calculation of the first $\mathfrak{D}'(k, k_0)$ and second $\mathfrak{D}''(k, k_0)$ partial derivatives of Eq. (36) or (38) with respect to k and k_0 for both EH and HE modes. During the solution of this problem, the period and constitutive parameters of the underlying materials of the superlattice are fixed, and the search for the effect manifestation is realized by altering the filling factors δ_m and δ_s within the period. The found crossing points are depicted in **Figure 8a** and **b** by green circles. We should note that in both configurations, the degeneracy points for EH (red line) and HE (blue line) surface polaritons can be obtained only for the case of composite structure with a predominant impact of the semiconductor subsystem. In particular, this state is found out to be at the values of filling factor $\delta_m = 0.27$ and $\delta_m = 0.15$ for the polar and Faraday configurations, respectively. Remarkable, in the Faraday geometry, both dispersion curves possess an anomalous dispersion line, namely, they start on the light line and fall just to the right of the light line, and then they flatten out and approach an asymptotic limit for large values of k. Contrariwise to the Faraday geometry, in the polar geometry, both dispersion curves demonstrate normal dispersion.

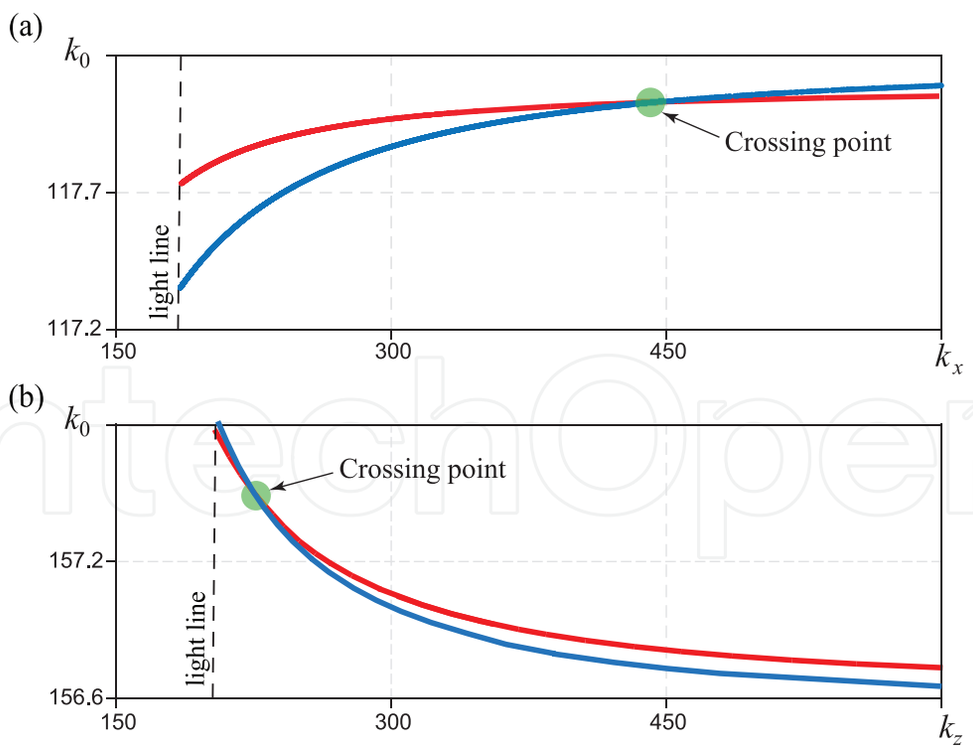

Figure 8. Manifestation of the crossing effect in dispersion curves of hybrid EH (red line) and HE (blue line) surface polaritons; (a) polar configuration ($\delta_m = 0.27$) and (b) Faraday configuration ($\delta_m = 0.15$). All structure constitutive parameters are shown in **Figure 2**.

6. Conclusions

To conclude, in this chapter, we have studied dispersion features of both bulk and surface polaritons in a magnetic-semiconductor superlattice influenced by an external static magnetic field. The investigation was carried out under an assumption that all characteristic dimensions of the given superlattice satisfy the long-wavelength limit; thus, the homogenization procedures from the effective medium theory was involved, and the superlattice was represented as a gyroelectromagnetic uniform medium characterized by the tensors of effective permeability and effective permittivity.

The general theory of polaritons in the gyroelectromagnetic medium whose permittivity and permeability simultaneously are tensor quantities was developed. Three particular configurations of the magnetization, namely, the Voigt, polar, and Faraday geometries, were discussed in detail.

The crossing and anti-crossing effects in the dispersion curves of both surface and bulk polaritons have been identified and investigated with an assistance of the analytical theory about the Morse critical points.

We argue that the discussed dispersion features of polaritons identified in the magnetic-semiconductor superlattice under study have a fundamental nature and are common to different types of waves and waveguide systems.

Author details

Vladimir R. Tuz[1,2], Illia V. Fedorin[3] and Volodymyr I. Fesenko[1,2]*

*Address all correspondence to: volodymyr.i.fesenko@gmail.com

1 International Center of Future Science, State Key Laboratory on Integrated Optoelectronics, College of Electronic Science and Engineering, Jilin University, China

2 Institute of Radio Astronomy of National Academy of Sciences of Ukraine, Ukraine

3 National Technical University 'Kharkiv Polytechnical Institute', Ukraine

References

[1] Agranovich VM, Ginzburg V. Crystal optics with spatial dispersion, and excitons. Berlin: Springer. 1984;**XI**:447. DOI: 10.1007/978-3-662-02406-5

[2] Ozbay E. Plasmonics: Merging photonics and electronics at nanoscale dimensions. Science. 2006;**311**(5758):189-193. DOI: 10.1126/science.1114849

[3] Armelles G, Cebollada A, Garcia-Martin A, Ujue Gonzalez M. Magnetoplasmonics: Combining magnetic and plasmonic functionalities. Advanced Optical Materials. 2013;**1**(1): 10-35. DOI: 10.1002/adom.201200011

[4] Anker JN, Hall WP, Lyandres O, Shah NC, Zhao J, Van Duyne RP. Biosensing with plasmonic nanosensors. Nature Materials. 2008;**7**:442-453. DOI: 10.1038/nmat2162

[5] Jun YC. Electrically-driven active plasmonic devices. In: Ki YK, editor. Plasmonics - Principles and Applications. InTech: Rijeka; 2012. pp. 383-400. DOI: 10.5772/50756

[6] Dicken MJ, Sweatlock LA, Pacific D, Lezec HJ, Bhattacharya K, Atwater HA. Electrooptic modulation in thin film barium titanate plasmonic interferometers. Nano Letters. 2008; **8**(11):4048-4052. DOI: 10.1021/nl802981q

[7] Min C, Wang P, Jiao X, Deng Y, Ming H. Beam manipulating by metallic nano-optic lens containing nonlinear media. Optics Express. 2007;**15**(15):9541-9546. DOI: 10.1364/OE.15.009541

[8] Hu B, Zhang Y, Wang QJ. Surface magneto plasmons and their applications in the infrared frequencies. Nanophotonics. 2015;**4**(1):383-396. DOI: 10.1515/nanoph-2014-002

[9] Kaganov MI, Pustyl'nik NB, Shalaeva TI. Magnons, magnetic polaritons, magnetostatic waves. Physics-Uspekhi. 1997;**40**(2):181-224. DOI: 10.1070/PU1997v040n02ABEH000194

[10] Wallis RF, Brion JJ, Burstein E, Hartstein A. Theory of surface polaritons in anisotropic dielectric media with application to surface magnetoplasmons in semiconductors. Physical Review B. 1974;**9**(8):3424-3343. DOI: 10.1103/PhysRevB.9.3424

[11] Camley RE, Mills DL. Surface polaritons on uniaxial antiferromagnets. Physical Review B. 1982;**26**(3):1280-1287. DOI: 10.1103/PhysRevB.26.1280

[12] Abraha K, Smith SRP, Tilley DR. Surface polaritons and attenuated total reflection spectra of layered antiferromagnets in the Faraday configuration. Journal of Physics: Condensed Matter. 1995;**7**(32):6423-6436. DOI: 10.1088/0953-8984/7/32/008

[13] Elmzughi FG, Constantinou NC, Tilley DR. Theory of electromagnetic modes of a magnetic superlattice in a transverse magnetic field: An effective-medium approach. Physical Review B. 1995;**51**(17):11515-11520. DOI: 10.1103/PhysRevB.51.11515

[14] Kushwaha MS. Plasmons and magnetoplasmons in semiconductor heterostructures. Surface Science Reports. 2001;**41**(1):1-416. DOI: 10.1016/S0167-5729(00)00007-8

[15] Abraha K, Tilley DR. The theory of far-infrared optics of layered antiferromagnets. Journal of Physics: Condensed Matter. 1995;**7**(14):2717

[16] Askerbeyli RT (Tagiyeva). The influence of external magnetic field on the spectra of magnetic polaritons and magnetostatic waves. Journal of Superconductivity and Novel Magnetism. 2016;**30**(4):1115-1122. DOI: 10.1007/s10948-016-3869-4

[17] Datta S, Furdyna JK, Gunshor RL. Diluted magnetic semiconductor superlattices and heterostructures. Superlattices and Microstructures. 1985;**1**(4):327-334. DOI: 10.1016/0749-6036(85)90094-1

[18] Munekata H, Zaslavsky A, Fumagalli P, Gambino RJ. Preparation of (In,Mn)As/(Ga,Al)Sb magnetic semiconductor heterostructures and their ferromagnetic characteristics. Applied Physics Letters. 1993;**63**(21):2929-2931. DOI: 10.1063/1.110276

[19] Koshihara S, Oiwa A, Hirasawa M, Katsumoto S, Iye Y, Urano C, et al. Ferromagnetic order induced by photogenerated carriers in magnetic III-V semiconductor heterostructures of (In, Mn)As/GaSb. Physical Review Letters. 1997;**78**(24):4617-4620. DOI: 10.1103/PhysRevLett.78.4617

[20] Ta JX, Song YL, Wang XZ. Magneto-phonon polaritons in two-dimension antiferromagnetic/ion-crystalic photonic crystals. Photonics and Nanostructures: Fundamentals and Applications. 2012;**10**(1):1-8. DOI: 10.1016/j.photonics.2011.05.007

[21] Jungwirth T, Sinova J, Masek J, Kucera J, MacDonald AH. Theory of ferromagnetic (III, Mn)V semiconductors. Reviews of Modern Physics. 2006;**78**(3):809-864. DOI: 10.1103/RevModPhys.78.809

[22] Polo JA, Mackay TG, Lakhtakia A. Electromagnetic surface waves. A modern perspective. London: Elsevier; 2013. 293 p

[23] Bass FG, Bulgakov AA. Kinetic and electrodynamic phenomena in classical and quantum semiconductor superlattices. New York: Nova Science. 1997

[24] Agranovich VM. Dielectric permeability and influence of external fields on optical properties of superlattices. Solid State Communications. 1991;**78**(8):747-750. DOI: 10.1016/0038-1098(91)90856-Q

[25] Eliseeva SV, Sementsov DI, Stepanov MM. Dispersion of bulk and surface electromagnetic waves in bigyrotropic finely stratified ferrite-semiconductor medium. Technical Physics. 2008;**53**(10):1319-1326. DOI: 10.1134/S1063784208100101

[26] Tuz VR. Polaritons dispersion in a composite ferrite-semiconductor structure near gyrotropic-nihility state. Journal of Magnetism and Magnetic Materials. 2016;**419**: 559-565. DOI: 10.1016/j.jmmm.2016.06.070

[27] Tuz VR. Gyrotropic-nihility state in a composite ferrite-semiconductor structure. Journal of Optic. 2015;**17**(3). DOI: 035611, 10.1088/2040-8978/17/3/035611

[28] Tuz VR, Fesenko VI. Gaussian beam tunneling through a gyrotropic-nihility finely-stratified structure. In: Shulika OV, Sukhoivanov IA, editors. Contemporary Optoelectronics. Netherlands: Springer; 2016. pp. 99-113. DOI: 10.1007/978-94-017-7315-7

[29] Collin RE. Foundation for Microwave Engineering. New Jersey: Wiley-Interscience; 1992

[30] Rui-Xin Wu, Tianen Zhao, John Q Xiao. Periodic ferrite-semiconductor layered composite with negative index of refraction. Journal of Physics: Condensed Matter. 2007;**19**(2): 026211. DOI: 10.1088/0953-8984/19/2/026211

[31] Shestopalov VP. Morse critical points of dispersion equations. Soviet Physics Doklady. 1990;**35**:905

[32] Shestopalov VP. Morse critical points of dispersion equations of open resonators. Electromagnetics. 1993;**13**:239-253. DOI: 10.1080/02726349308908348

[33] Yakovlev AB, Hanson GW. Analysis of mode coupling on guided-wave structures using Morse critical points. IEEE Transactions on Microwave Theory and Techniques. 1998;**46**(7): 966-974. DOI: 10.1109/22.701450,

[34] Yakovlev AB, Hanson GW. Mode-transformation and mode-continuation regimes on waveguiding structures. IEEE Transactions on Microwave Theory and Techniques. 2000;**48**(1):67-75. DOI: 10.1109/22.817473

[35] Yakovlev AB, Hanson GW. Fundamental wave phenomena on biased-ferrite planar slab waveguides in connection with singularity theory. IEEE Transactions on Microwave Theory and Techniques. 2003;**51**(2):583-587. DOI: 10.1109/TMTT.2002.807809

[36] Gilmore R. Catastrophe Theory for Scientists and Engineers. New York: Wiley; 1981

[37] Ibanescu M, Johnson SG, Roundy D, Luo C, Fink Y, Joannopoulos JD. Anomalous dispersion relations by symmetry breaking in axially uniform waveguides. Physical Review Letters. 2004;**92**(6):063903. DOI: 10.1103/PhysRevLett.92.063903

[38] Ivanov ST. Waves in bounded magnetized plasmas. In: Schluter H, Shivarova A, editors. Advanced Technologies Based on Wave and Beam Generated Plasmas. Netherlands: Springer; 1999. pp. 367-390

[39] Fesenko VI, Fedorin IV, Tuz VR. Dispersion regions overlapping for bulk and surface polaritons in a magnetic-semiconductor superlattice. Optics Letters. 2016;**41**(9):2093-2096. DOI: 10.1364/OL.41.002093

[40] Tarkhanyan RH, Niarchos DG. Effective negative refractive index in ferromagnet-semiconductor superlattices. Optics Express. 2006;**14**(12):5433-5444. DOI: 10.1364/OE.14.005433

[41] Tarkhanyan RH, Niarchos DG. Influence of external magnetic field on magnon-plasmon polaritons in negative-index antiferromagnet-semiconductor superlattices. Journal of Magnetism and Magnetic Materials. 2010;**322**(6):603-608. DOI: 10.1016/j.jmmm.2009.10.023

[42] Tuz VR, Fesenko VI, Fedorin IV, Sun H-B, Han W. Coexistence of bulk and surface polaritons in a magnetic-semiconductor superlattice influenced by a transverse magnetic field. Journal of Applied Physics. 2017;**121**(10):103102. DOI: 10.1063/1.4977956

[43] Ginzburg VL. The Propagation of Electromagnetic Waves in Plasma. London: Gordon and Breach; 1962

[44] Tuz VR, Fesenko VI, Fedorin IV, Sun H-B, Shulga VM. Crossing and anti-crossing effects of polaritons in a magnetic-semiconductor superlattice influenced by an external magnetic field. Superlattices and Microstructures. 2017;**103**:285-294. DOI: 10.1016/j.spmi.2017.01.040

[45] Brion JJ, Wallis RF. Theory of pseudosurface polaritons in semiconductors in magnetic fields. Physical Review B. 1974;**10**(8):3140-3143. DOI: 10.1103/PhysRevB.10.3140

IntechOpen